

# Thermally Responsive Hydrogels for Passive Temperature Regulation under Direct Sunlight

Dajie Xie, Wei Li, Corey A. Richards, Haibo Gao, Chen Chen, Nenad Miljkovic, Shanhui Fan, Jae Lee, Shailesh N. Joshi, and Paul V. Braun\*

By spontaneously emitting midinfrared radiation to outer space through the atmospheric window and reflecting sunlight, daytime radiative coolers achieve notable passive cooling performance. However, existing daytime radiative cooling systems generally lack the ability to adaptively switch between heating and cooling states based on ambient conditions. Herein a passive thermal regulation system that features a temperature-dependent switchable solar reflectance from 0.05 (low temperature) to 0.8 (high temperature) is presented. This, along with a  $\approx 0.95$  midinfrared emittance, it enables automatic switching between radiative cooling and solar heating. Switchability is enabled using a poly(*N*-isopropylacrylamide) (PNIPAM) hydrogel which exhibits high solar scattering above its tunable lower critical solution temperature (LCST) and transparency below its LCST. The lower part of the hydrogel is loaded with graphite to absorb solar energy in the heating state. In testing under sunny and partly cloudy outside conditions, this system maintains a temperature close to the set LCST.

temperatures and populations expect to further increase the energy demand.<sup>[1,2]</sup> Passive thermal regulation technologies present a path toward the reduction of energy demands by heating or cooling surfaces without energy input. Daytime radiative cooling has been demonstrated to reduce active cooling demands during hot summer days. Cooling of  $\approx 5$  °C is achieved under direct sunlight by simultaneously reflecting solar radiation (0.3–2.5  $\mu\text{m}$ ) and dissipating heat to outer space through the midinfrared atmospheric window (8–13  $\mu\text{m}$ ).<sup>[3–11]</sup> However, most daytime radiative cooling systems cannot automatically switch from cooling to heating (solar absorbing) to provide net heating on cooler days or to maintain a surface at a near-constant temperature under varying solar irradiance and ambient temperatures.

Radiative cooling systems with switchable solar reflectance and/or midinfrared emittance enable passive thermal regulation through selective heating and cooling. Over the last few years, reports of actively switched radiation-based thermal regulation systems include mechanically actuated coatings,<sup>[12]</sup> porous polymer coatings with reversible wetting,<sup>[13]</sup>


## 1. Introduction

Building and mobile heating, ventilation, and air conditioning (HVAC) systems consume a significant amount of global energy to achieve human thermal comfort. Increases in global

D. Xie, C. A. Richards, H. Gao, C. Chen, P. V. Braun  
Department of Materials Science and Engineering  
Beckman Institute for Advanced Science and Technology  
University of Illinois Urbana-Champaign  
Urbana, IL 61801, USA  
E-mail: pbraun@illinois.edu

D. Xie, C. A. Richards, H. Gao, C. Chen, N. Miljkovic, P. V. Braun  
Materials Research Laboratory  
University of Illinois Urbana-Champaign  
Urbana, IL 61801, USA

W. Li, S. Fan  
E. L. Ginzton Laboratory  
Department of Electrical Engineering  
Stanford University  
Stanford, CA 94305, USA

 The ORCID identification number(s) for the author(s) of this article can be found under <https://doi.org/10.1002/adpr.202200253>.

© 2023 The Authors. Advanced Photonics Research published by Wiley-VCH GmbH. This is an open access article under the terms of the Creative Commons Attribution License, which permits use, distribution and reproduction in any medium, provided the original work is properly cited.

DOI: 10.1002/adpr.202200253

W. Li  
GPL Photonics Lab  
State Key Laboratory of Applied Optics  
Changchun Institute of Optics  
Fine Mechanics and Physics  
Chinese Academy of Sciences  
Changchun 130033, China

N. Miljkovic, P. V. Braun  
Department of Mechanical Science and Engineering  
University of Illinois Urbana-Champaign  
Urbana, IL 61801, USA

N. Miljkovic  
Department of Electrical and Computer Engineering  
University of Illinois Urbana-Champaign  
Urbana, IL 61801, USA

N. Miljkovic  
International Institute for Carbon-Neutral Energy Research (WPI-I2CNER)  
Kyushu University  
Nishi-ku 819-0395, Japan

J. Lee, S. N. Joshi  
Electronics Research Department  
Toyota Research Institute of North America  
Ann Arbor, MI 48105, USA

dual-mode thermal emitters,<sup>[14,15]</sup> and electrochromic devices.<sup>[16,17]</sup> Although thermal tuning is achieved by these systems, active intervention is required to actuate the switching. Passive thermal regulation systems that can automatically react to external stimuli to transition between heating and cooling states are therefore highly desired.

Materials that exhibit temperature-dependent optical properties have the potential to realize passive thermal regulation. Self-adaptive regulated radiative cooling systems containing phase-change materials, for example, vanadium oxide (VO<sub>2</sub>), were first theoretically<sup>[18–20]</sup> and, very recently, experimentally<sup>[21,22]</sup> demonstrated. The VO<sub>2</sub>-based system automatically switches midinfrared emittance via a metal–insulator transition which turns the radiative cooling on and off. However, the complexity of the designed structure and poor cyclability<sup>[23,24]</sup> of VO<sub>2</sub> limit real-world applications. In contrast, the poly(*N*-isopropylacrylamide) (PNIPAM) hydrogel exhibits excellent temperature-dependent whiteness due to its lower critical solution temperature (LCST) phenomenon and is widely studied for smart windows to regulate indoor temperature by switching between transmitting (below the LCST) and scattering (above the LCST) incoming sunlight.<sup>[25–27]</sup> Recent work<sup>[28,29]</sup> demonstrates a further enhancement of the regulation of indoor temperature by the addition of the potential of radiative cooling into the system.

Here, we design a temperature-tunable adaptive reflectance-switchable hydrogel radiator (ARSHR) using a poly(*N*-isopropylacrylamide) (PNIPAM) hydrogel as the foundational element that passively switches between solar heating and radiative cooling states depending on ambient temperature. The ARSHR exhibits an autonomic switchable solar reflectance from 0.05 (strongly absorbing) to 0.8 (strongly reflective) at a tunable temperature. The ARSHR exhibits a ≈0.95 midinfrared emittance regardless of temperature, enabling it to be an efficient thermal emitter. Using this system, we computationally and experimentally demonstrate that the ARSHR maintains a temperature around a defined point under a range of solar irradiances and ambient temperatures. This system can be scaled to large areas and is formed using only low-cost materials. Recent work<sup>[30]</sup> demonstrated the use of a similar thermochromic hydrogel sandwiched between a polymer emitter and a metallic absorber to maintain thermal homeostasis around a single temperature, a related concept as we utilize. There are a number of important distinctions between that and our report including that we perform what we suggest is a more complete optical analysis; in the previous report the thermal emitter, hydrogel, and absorber are separate elements, while in our system all components are integrated, our system exhibits a tunable temperature setpoint while the previous report does not, and our system is demonstrated to be stable over many cycles, including to below freezing temperatures while the previous report did not discuss cycling or freezing, which of course would occur in a real-world environment.

## 2. Results and Discussion

### 2.1. Principle and Fabrication Process of ARSHR

The passive thermal regulation achieved by our ARSHRs can be quantitatively analyzed through the well-established relationship<sup>[4]</sup>

between the thermal radiation from the emitter ( $P_{\text{rad}}$ ), the thermal radiation absorbed by the atmosphere ( $P_{\text{atm}}$ ), and absorbed thermal radiation from sunlight ( $P_{\text{solar}}$ ).

$$P_{\text{net}} = P_{\text{rad}}(T) - P_{\text{atm}}(T_{\text{amb}}) - P_{\text{solar}}(T, I_{\text{solar}}, \text{LCST}) \quad (1)$$

where  $T$  is the emitter temperature,  $T_{\text{amb}}$  is the ambient temperature, and  $I_{\text{solar}}$  is the solar irradiance. The nonradiative heat transfer, that is, conduction and convection, is neglected in our analysis. The tunability of our system arises from the unique dependence of  $P_{\text{solar}}$  on the LCST of the PNIPAM hydrogel,<sup>[31,32]</sup> above which phase separation between water and PNIPAM chains reversibly occurs, leading to significant light scattering.

As shown in **Figure 1a**, the ARSHR comprises a PNIPAM hydrogel consisting of a graphite-free layer above an absorptive graphite-loaded layer. At high temperature ( $T > \text{LCST}$ ), the PNIPAM hydrogel undergoes phase separation into polymer-rich and water-rich phases, causing strong solar scattering<sup>[25,33,34]</sup> and thus the bilayer appears white (**Figure 1b**, left). The solar reflectance of a PNIPAM hydrogel at 50 °C ( $\text{LCST} \approx 32$  °C) is plotted in **Figure 1c**, demonstrating the ARSHR's ability to reduce  $P_{\text{solar}}$  above the LCST. Coupled with its ≈0.95 midinfrared emittance (**Figure 1d**), originating from the strong absorption of the hydrogen bond bending and stretching in water,<sup>[35]</sup> the ARSHR is in an efficient cooling state ( $P_{\text{net}} > 0$ ).

At lower temperature ( $T < \text{LCST}$ ), the top layer is single phase (**Figure 1a**, right) and thereby optically transparent, allowing sunlight to be absorbed by the bottom graphite-loaded layer (**Figure 1b**, right). The solar reflectance of the top layer is low (**Figure 1c**), whereas the midinfrared emittance remains high (**Figure 1d**), turning the ARSHR into an efficient solar heater ( $P_{\text{net}} < 0$ ) as the solar irradiance is typically much stronger than the radiative cooling ( $P_{\text{solar}} \gg P_{\text{rad}} - P_{\text{atm}}$ ).

The bilayer hydrogel is synthesized by simple free radical polymerization at room temperature. Briefly, NIPAM monomer, crosslinker, initiator, and graphite powders are dissolved in deionized (DI) water to form the precursor solution. After catalyst addition, the solution is cast as a layer which polymerizes forming a graphite-loaded hydrogel. Then, a graphite-free hydrogel precursor solution is cast on the graphite-containing layer via the same procedure, resulting in a stable bilayer hydrogel. The two layers are tightly bonded because of the formation of an interpenetrating-network at the interface.<sup>[36]</sup> Finally, the bilayer ARSHR is sealed between low-density polyethylene (LDPE) films to prevent water evaporation. The LDPE does not affect the optical performance of ARSHRs due to its high solar and midinfrared transparency (**Figure S1**, Supporting Information). Important for application, the ARSHR consists of low-cost materials.

### 2.2. Characterization of the PNIPAM Hydrogel

To investigate the temperature-dependent microstructure of the PNIPAM polymer, PNIPAM hydrogels equilibrated at 25 and 50 °C were shock frozen in liquid nitrogen and then freeze dried to preserve the polymer network morphology. Scanning electron microscopy (SEM) images show that the hydrogel below the LCST only contains pores smaller than 100 nm (**Figure 2a**),

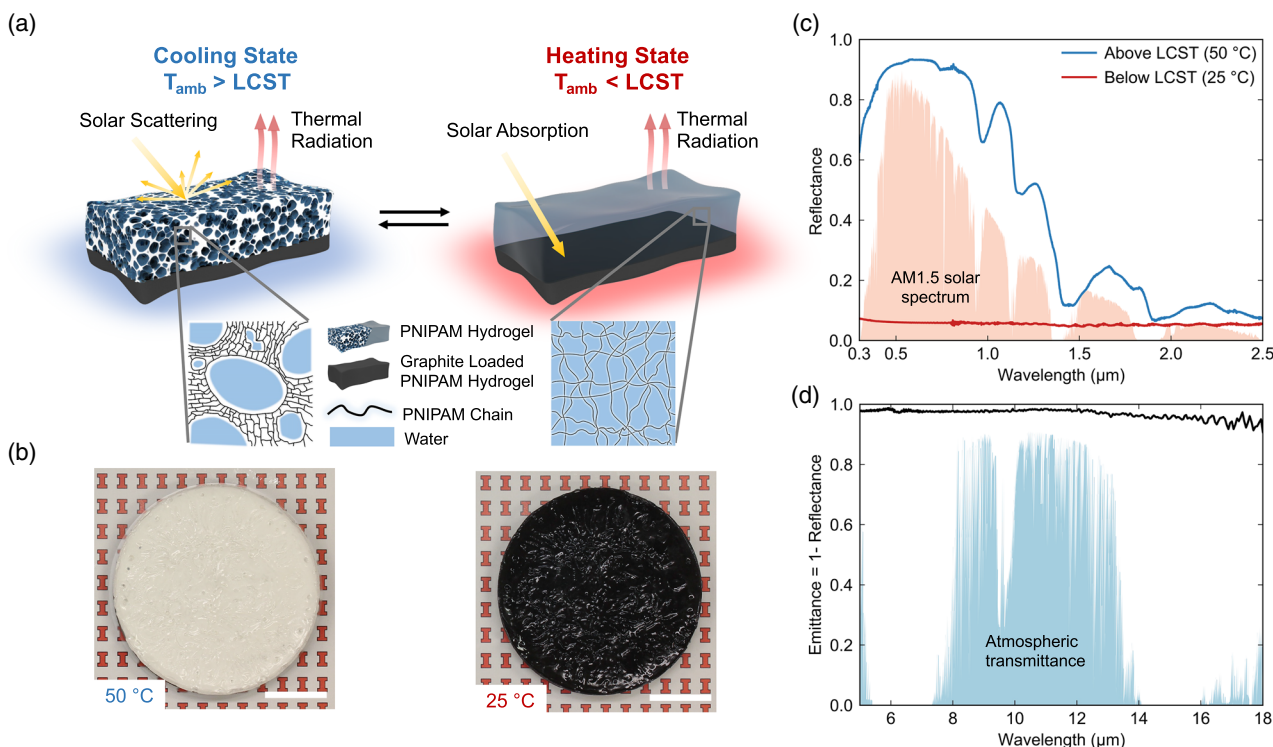


**Figure 1.** Adaptively switchable hydrogel system for passive heating and cooling. a) Schematic of the hydrogel bilayer illustrating its cooling and heating states. As the temperature decreases, the top PNIPAM hydrogel layer automatically switches between a phase-separated state (solar scattering) and a homogeneous transparent state, which allows solar radiation to reach the bottom graphite-loaded hydrogel. Schematics not to scale. b) Photos of the hydrogel bilayer (LCST =  $\approx 32$  °C) at 50 °C (White) and 25 °C (Black). Scale bars: 4 cm. c) Solar reflectance spectrum of the hydrogel bilayer above the hydrogel LCST (50 °C) and below the hydrogel LCST (25 °C) with the solar AM 1.5 solar spectrum overlain in the background (arbitrary units). d) Infrared emittance spectrum of the hydrogel bilayer at 25 °C (emittance above LCST remains similar) with the atmospheric transmittance spectrum in the background (arbitrary units).

which we suspect are an artifact of the freezing and drying sample preparation process. Above the LCST, the polymer phase exhibits pores ranging from sub-100 nm to  $\approx 3$   $\mu\text{m}$  in diameter, confirming the significant phase separation (Figure 2b). Such a hierarchically porous structure will strongly scatter sunlight.<sup>[6,12]</sup>

To optimize the cooling performance of the ARSHR at high temperatures, it is necessary to maximize the solar reflectance above the LCST. Due to the high extinction coefficient of PNIPAM and water in the UV and NIR regimes<sup>[37,38]</sup> (Figure S2, Supporting Information), originating from the electronic transition absorption<sup>[39]</sup> and molecular vibrational absorption,<sup>[40]</sup> respectively, the PNIPAM hydrogel inevitably absorbs solar irradiance in those regimes (Figure 1c). When the thickness of the hydrogel is 6 mm, the reflectance above the LCST in the visible spectrum (300–800 nm) is  $>0.9$  and the spectrally averaged solar reflectance (300 nm–2.5  $\mu\text{m}$ ) is 0.8. The solar reflectance below the LCST remains 0.05, ensuring that the majority of solar radiation is transmitted to the absorber. Although the scattering-induced solar reflectance above the LCST is not sufficient to realize subambient temperature cooling, the high reflectance contrast ( $\approx 0.75$ ) provided by the ARSHR enables effective temperature regulation.

The LCST determines the temperature where the ARSHR switches between the heating and cooling state and thereby

controls the steady-state temperature. The LCST of PNIPAM in water is 32–35 °C and can be tuned by adding salts<sup>[41,42]</sup> and solvents<sup>[43,44]</sup> to the water phase, or via chemical modification of the polymer.<sup>[45]</sup> Here, to modulate the ASRRH regulation temperature, we added NaCl into the hydrogel films (see Experimental Section). The dissolved NaCl destabilizes hydrogen bonding between the polymer and water, lowering the LCST.<sup>[42]</sup> To measure the effect of NaCl on the LCST, the reflectance at 600 nm of PNIPAM hydrogel films containing varying concentrations of NaCl is measured as a function of temperature. As shown in Figure 2d, the LCST, determined at 50% normalized reflectance, reduces from  $\approx 32$  to  $\approx 22$  °C as the NaCl concentration increases from 0 (pure water) to 1 M. Differential scanning calorimetry (DSC) measurements confirm that the thermal hysteresis of the PNIPAM hydrogel is only about 1 °C (Figure S3, Supporting Information). Importantly, the solar reflectance of the PNIPAM hydrogel above and below the LCST does not change with salt concentration (Figure S4, Supporting Information), indicating that using only one starting material system, the temperature response of the ARSHR can be tuned as required for various applications.

Important for application is the cycling stability of the ARSHR. A PNIPAM hydrogel film (thickness = 1.5 mm) was repeatedly heated and cooled with temperature and



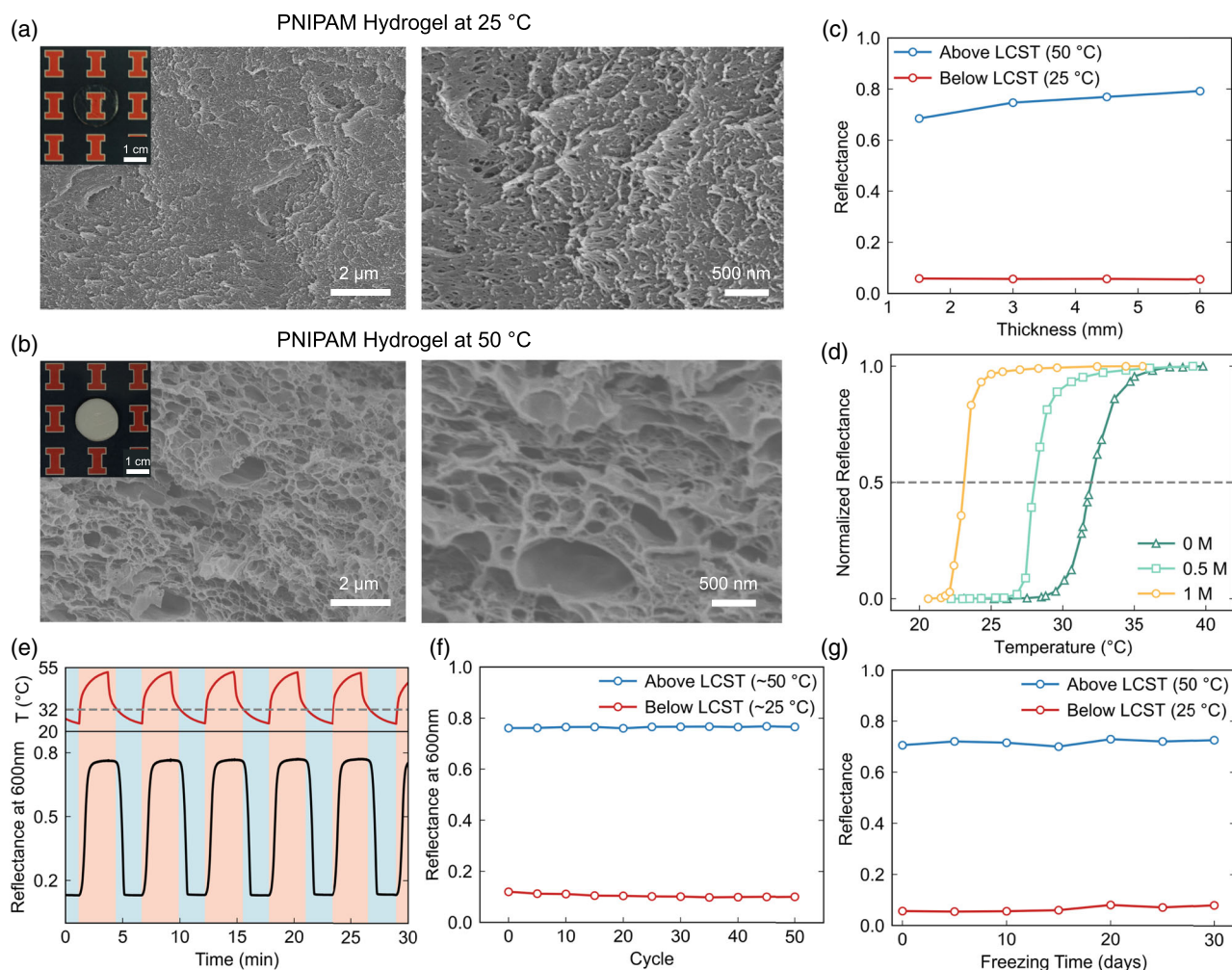


**Figure 2.** Morphology and optical switching properties of the PNIPAM hydrogel. a,b) SEM images of the PNIPAM hydrogel quenched below (25 °C) and above (50 °C) the LCST. Insets: Photographs of the PNIPAM hydrogel below (25 °C) and above (50 °C) the LCST. The PNIPAM hydrogel undergoes phase separation from a solid (transparent) to a porous (white) state when the temperature is increased above the LCST. c) Solar reflectance of the PNIPAM hydrogel as a function of thickness above (50 °C) and below (25 °C) the LCST. d) Normalized reflectance at 600 nm of the PNIPAM hydrogel containing the indicated concentration of NaCl as a function of sample temperature. The intersect with the dashed gray line (0.5 reflectance) demarks the LCST. e) Hydrogel reflectance and temperature during heating and cooling cycles as a function of time. f) Measured reflectance above ( $\approx 50$  °C) and below ( $\approx 25$  °C) the LCST over 50 thermal cycles. g) Average solar reflectance above (50 °C) and below (25 °C) the LCST after multiple freezing events for the indicated time. No degradation in optical performance is observed during cycling.

reflectance recorded simultaneously. The PNIPAM hydrogel quickly undergoes phase separation from a transparent to a reflective state as temperature rises above the LCST and recovers transparency once the temperature drops below the LCST (Figure 2e). The switching time is less than 1 min. The film only shows a negligible fluctuation of reflectance over more than 50 cycles (Figure 2f). To test the stability of this system to freezing conditions, the PNIPAM hydrogel film was frozen for 5 days at  $\approx -20$  °C and then melted at room temperature (25 °C), followed by the measurement of the solar reflectance above and below the LCST. The freezing and melting processes were repeated several times on the same film and the optical switchability remains unchanged (Figure 2g), indicating that freezing did not affect the optical properties of the hydrogel.

### 2.3. Thermal Regulation Performance Analysis of the ARSHR

Based on the measured spectral properties of the ARSHR components, we calculate the net cooling power of an ARSHR having an LCST of 32 °C under  $T_{\text{amb}} = 15$  °C and variable solar irradiance using Equation (1) (Figure 3a). When the ARSHR temperature is below the LCST, the ARSHR is in the solar heating state ( $P_{\text{net}} < 0$ ) and presents a heating power  $> 300 \text{ W m}^{-2}$  even when the ARSHR temperature is only 2 °C below the hydrogel LCST. This heating power will rapidly increase the ARSHR temperature above the LCST, transitioning it to its cooling state. When the ARSHR temperature is significantly above the LCST, the ARSHR is in the cooling state ( $P_{\text{net}} > 0$ ), and the ARSHR temperature reduces. The system reaches a steady-state temperature, defined as the solution of Equation (1) with  $P_{\text{net}}(T) = 0$ .

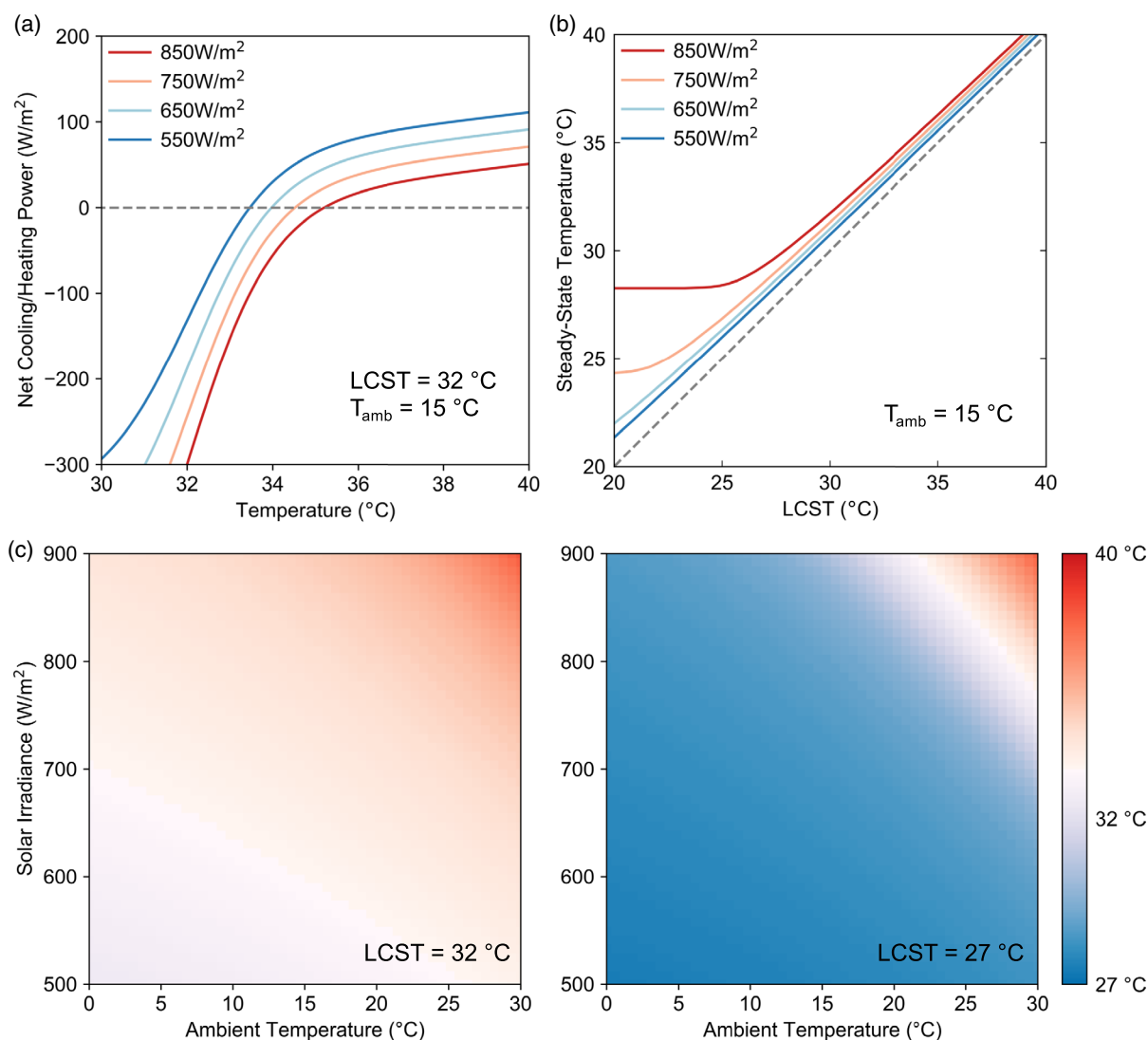


**Figure 3.** Calculated thermal regulation performance of the ARSHR. a) Net cooling/heating power of the ARSHR (LCST = 32 °C) as a function of the ARSHR temperature for  $T_{\text{amb}} = 15$  °C and a variety of solar irradiances. Strong heating powers ( $P_{\text{net}} < 0 \text{ W m}^{-2}$ ) are established when the temperature is below the LCST. Net cooling powers are observed ( $P_{\text{net}} > 0 \text{ W m}^{-2}$ ) when the temperature is significantly higher than the LCST. The intersects with the dashed gray line ( $P_{\text{net}} = 0 \text{ W m}^{-2}$ ) indicate the steady-state temperature. b) Steady-state temperature of the ARSHR as a function of the LCST for a variety of solar irradiances at  $T_{\text{amb}} = 15$  °C. The dashed gray line is the LCST. c) Steady-state temperature of ARSHRs as a function of the ambient temperature and solar irradiance when designed with hydrogels with the indicated LCST temperatures (LCST = 32 and 27 °C).

To quantitatively present the impact of LCST on the ARSHR performance, the steady-state temperature as a function of LCST is plotted in Figure 3b. The ARSHR maintains its steady-state temperatures only slightly above the set LCSTs, especially for weaker solar irradiance. Note that the PNIPAM hydrogel absorbs  $\approx 20\%$  of the solar irradiance even in the cooling state. Therefore, under strong solar irradiance, the ARSHR with relatively low LCST equilibrates at a higher temperature, providing a higher radiative cooling power to balance the absorbed heating power. In Figure 3c, the steady-state temperatures of the ARSHRs under different environmental conditions (ambient temperature, solar irradiance) are presented. The ARSHR (LCST = 32 °C) maintains steady-state temperatures within 3 °C above the LCST under large variance of ambient temperature (0–30 °C) and solar

irradiance (500–900 W m<sup>-2</sup>). Our theoretical calculation indicates that the ARSHR has the capability to regulate its temperature during all seasons and in most climates.

Due to intrinsic UV and NIR absorption of the PNIPAM hydrogel, the current ARSHR does not fully regulate temperature under the combination of high ambient temperature and strong solar radiation. We calculate that an ideal ARSHR with switchable solar reflectance from 0 to 1 near the transition temperature would maintain a temperature less than 1 °C above the set LCST regardless of the environmental conditions (Figure S5 and S6, Supporting Information). Future efforts need to focus on increasing the solar reflectance in the cooling state. One potential solution would be to develop alternative chemistries with lower NIR absorption. Replacing water with D<sub>2</sub>O would result in lower

NIR absorption<sup>[46]</sup> as the NIR vibrational absorption peaks of D<sub>2</sub>O shift to higher wavelengths. Another solution would be to add a filter designed using multilayer optical films,<sup>[47]</sup> which is optimized to only reflect UV and NIR light, to improve the overall solar reflectance.

## 2.4. Outdoor Performance of ARSHRs

To verify the thermal regulation performance of the system, continuous outdoor measurements of ARSHRs with LCSTs of  $\approx 32$  and  $\approx 27$  °C were carried out on clear and partly cloudy days in Champaign, IL, USA (40.11°N, 88.24°W). A static solar absorber and a daytime radiative cooler were tested simultaneously as controls. The solar absorber is obtained by placing the ARSHR upside down with the dark graphite-loaded hydrogel layer facing the incoming sunlight; this layer shows negligible solar reflectance change with temperature (Figure S7, Supporting Information). The daytime radiative cooling system consists of a 3M enhanced solar reflective film on Al foil (0.943 solar reflectance and  $\approx 0.95$  midinfrared emittance) to enable daytime radiative cooling (Figure S8, Supporting Information). All test samples were placed in a system designed to minimize effects of the surrounding environment (Figure 4a,b).

During night time, all samples showed similar radiative cooling abilities and cooled by  $\approx 5$  °C below the ambient temperature

due to their high midinfrared emittance (Figure 4b, inset). As the sun rises, the temperatures of the ARSHRs and solar absorber began to increase at similar rates while the daytime radiative cooler remained close to the ambient temperature. Turnover points are clearly observed in the temperature profiles of the ARSHRs, as they transition from the heating to the cooling stages. Remarkably, the ARSHRs quickly stabilize at an average temperature of 28.9 °C (LCST =  $\approx 27$  °C) and 35.8 °C (LCST =  $\approx 32$  °C) within  $\approx 10$  °C of the ambient temperature at an average solar irradiance of  $\approx 500$  W m<sup>-2</sup> from shortly after sunrise to near sunset (Figure 4c). The low LCST ARSHR temperature curve exhibits a more abrupt transition, caused by the steeper phase transition around the LCST (Figure 2d). The simple solar absorber heated up to around 60 °C while the daytime radiative cooler remained close to the ambient temperature. Note, due to the solar illumination and heat trapped within the enclosed test chamber, the ambient temperature inside the chamber slightly increased at noontime (Figure S9, Supporting Information), and thereby the daytime radiative cooler used here does not achieve subambient temperature cooling. Rooftop experiments were also conducted on the partly cloudy days demonstrating that the ARSHRs still maintain a temperature near the set LCST (Figure S10, Supporting Information).

We suggest that implementing the ARSHR in applications requiring year-round temperature control can reduce annual

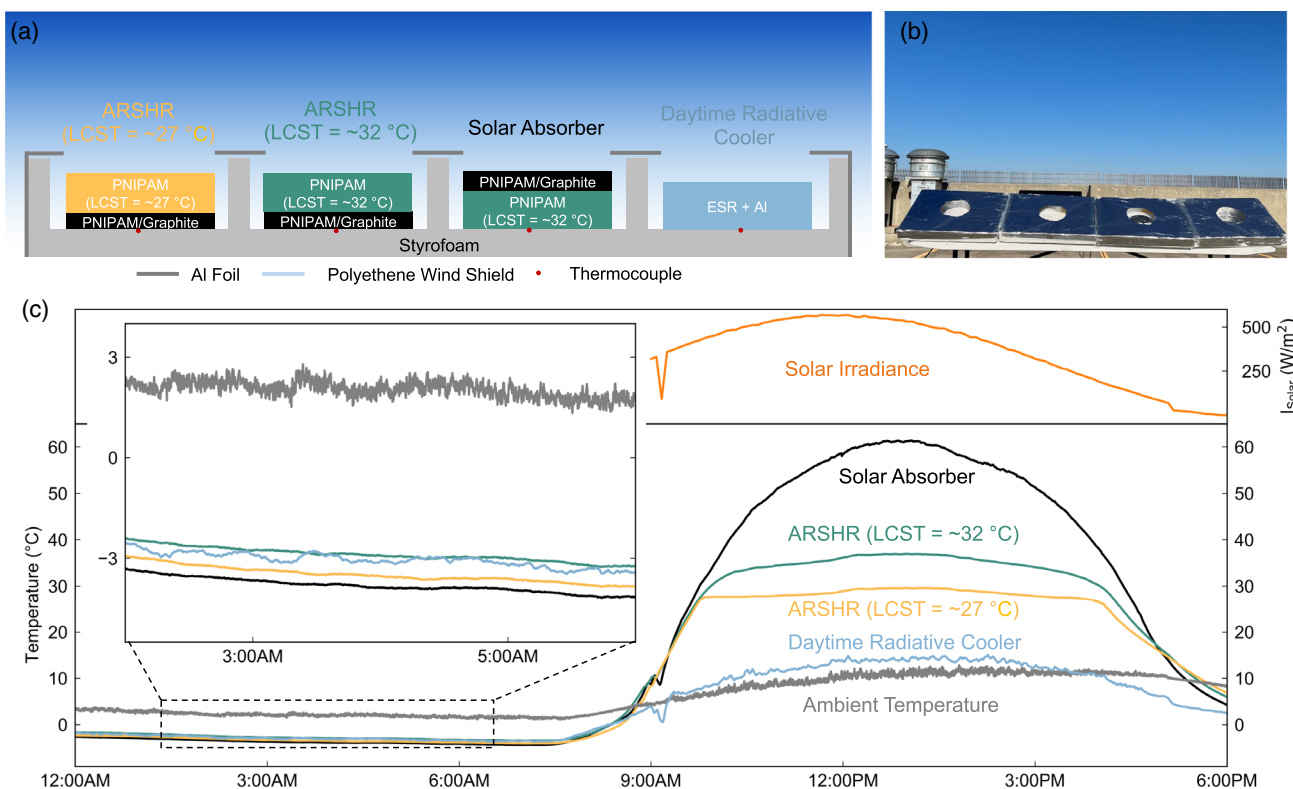


**Figure 4.** Outdoor temperature measurement of ARSHRs. a) Schematic of the measurement apparatus and test samples. In addition to the ARSHRs with LCST of  $\approx 27$  and  $\approx 32$  °C, a static solar absorber and a daytime radiative cooler were tested simultaneously as control samples. Schematics not to scale. b) Photograph of the temperature measurement experiments conducted on a clear day on a building rooftop in Champaign, IL, USA. c) Temperature measurements of the ARSHRs, static solar absorber, and daytime radiative cooler over a day cycle. Insets show the night-time temperatures of the samples when compared to the ambient temperature. Temperature measurement uncertainties are  $\pm 0.5$  °C and are not shown for clarity.

energy consumption. It has been reported that switching from solar absorbing black to solar reflective white paints in buildings and vehicles can result in  $\approx 20\text{--}40\%$  energy savings for indoor human thermal comfort,<sup>[48,49]</sup> especially during the summer months. The bilayer hydrogel system, with adaptive solar reflectance that both reduces the heat gain in summer and heat loss in winter, would further increase these energy savings. Daytime radiative cooling systems can also potentially be coupled with air-conditioning systems to improve cooling performance.<sup>[50]</sup> Reversible heat pump systems coated with the ARSHR on the outdoor heat exchanger have potential for higher year-round efficiency. In addition, the passive temperature regulation provided by the ARSHR may even potentially benefit personal thermal management technologies by assisting in the maintenance of a more uniform body temperature. To enable a long period of use, the addition of UV stabilizers and antimicrobial agents may be required. Such experiments were outside of the scope of this study.

### 3. Conclusion

Here, we report ARSHRs for passive thermal regulation based on the tunable LCST phenomenon of thermally responsive PNIPAM. This system possesses switchable solar reflectance from 0.05 to 0.8 at an adjustable LCST and  $\approx 0.95$  midinfrared emittance, enabling it to maintain temperature near the LCST set point. Real-time temperature measurements and theoretical calculations verify the temperature regulation capability for different ambient temperatures and solar irradiances. Our materials system is formed through a facile fabrication method using only low-cost materials and exhibits excellent cycling stability as well as durability to freezing environment, important characteristics for real-world applicability. This work demonstrates the viability of passive temperature control under a range of environmental conditions and demonstrates a potential material system for autonomic seasonal thermal regulation for reducing energy consumption in applications including buildings, vehicles, storage tanks, and reversible heat pumps.

### 4. Experimental Section

**Materials:** *N*-isopropylacrylamide (NIPAM, 99%), *N,N'*-methylenebisacrylamide (BIS, 99%), potassium persulfate (KPS, >99%), graphite powders, and *N,N,N',N'*-tetramethyl ethylenediamine (TEMED, 99%) were purchased from Sigma-Aldrich. Sodium chloride (NaCl) was purchased from Fisher Science.

**PNIPAM Hydrogel Fabrication:** In a typical procedure, the hydrogel precursor solution was prepared by dissolving 0.5 g of NIPAM monomer, 10 mg of BIS, and 10 mg of KPS in 4.5 mL of DI water. After purging with clean nitrogen gas in an ice bath for 30 min and adding 20  $\mu\text{L}$  of TEMED, the precursor solution was injected between two glass slides with a controlled separation at room temperature. The mixture was allowed to polymerize for 2 h, and the glass slides were removed, resulting in a hydrogel film of defined thickness. To change the LCST, the resulting hydrogel film was incubated in 0.5 or 1 M NaCl solutions at 50 °C for 60 min and then incubated in a fresh NaCl solution of the same concentration at 25 °C for 60 min. This process was repeated three times to ensure the ion exchange within the film.

**ARSHR Fabrication:** To prepare the bottom graphite-loaded hydrogel layer, 4 g NIPAM, 80 mg BIS, 80 mg KPS, and 200 mg graphite powders were added to 36 mL DI water to form the precursor solution.

After purging with nitrogen gas in an ice bath for 30 min, 160  $\mu\text{L}$  TEMED was added to the precursor solution. The precursor solution was then poured into a 15 cm-diameter circular glass mold and allowed to polymerize at room temperature for 2 h. Then, 100 mL of precursor solution without graphite powder was prepared and poured on top of the solidified bottom layer, forming the bilayer ARSHR. The thicknesses of the graphite-loaded hydrogel and pure hydrogel were measured to be  $\approx 2$  and  $\approx 6$  mm, respectively. The as-prepared bilayer ARSHR was removed from the mold and then sealed between two 15  $\mu\text{m}$ -thick LDPE films using a vacuum sealer machine (Enrigne, E2902-MS) to prevent water evaporation.

**Optical Measurements:** UV–vis–NIR reflectance spectra of the PNIPAM hydrogel films were measured using a UV–vis–NIR spectrometer (Agilent, Cary 5 G) equipped with an integrating sphere (Agilent, internal DRA 2500). To control the temperature of the sample, the sample was placed on a Peltier module (CUI Device, CP60240) and an adhesive thermocouple (Omega, SA1-KI-1M) was attached to the back side and connected to a data logger (Pico Technology, TC-08) to monitor the temperature. For the temperature-dependent reflectance measurement, the UV–vis–NIR spectrometer was operated in the kinetic mode and the reflectance at 600 nm was measured as a function of time. The reflectance, temperature, and time series were recorded simultaneously during the heating and cooling cycles. To measure the LCST, the reflectance was recorded 5 min after the Peltier module reached a certain temperature, ensuring thermal equilibrium of the hydrogel. The reflectance data were normalized for LCST determination. The midinfrared reflectance was measured using a Fourier-transform infrared (FTIR) spectrometer (Thermo, Nicolet Nexus 670) equipped with a gold integrating sphere (Pike, IntergatIR MIR). The midinfrared emittance was calculated by subtracting the measured reflectance from unity.

**SEM Characterization:** The PNIPAM hydrogel was equilibrated in DI water at 25 or 50 °C and then shock frozen in liquid nitrogen. The frozen hydrogel was freeze dried overnight using a benchtop freeze dryer (Labconco, FreeZone Legacy 2.5). The dry polymer samples were sputtered with an Au–Pd sputter coater (Emitech, K575) for 30 s and then imaged by SEM (Hitachi, S-4800).

**Thermal Measurements:** DSC (TA instrument, Discovery 2500) was performed to determine the LCST and the thermal hysteresis of the PNIPAM hydrogel. The scanning rate was 1.5 K min<sup>−1</sup> to ensure that the kinetics of water transport within the hydrogel during heating and cooling does not lead to an observed hysteresis.

**Rooftop Measurements:** The outdoor thermal regulation experiments were carried out on a building rooftop in Champaign, IL, USA, in November 2021. The apparatus consisted of a handmade Styrofoam chamber and all samples were mounted on the bottom of the chamber (Figure 4a). The apparatus top was covered by an LDPE film to minimize conduction and convection and then covered by Al foil with a window of the sample size to allow radiative heat exchange. Adhesive thermocouples (Omega, SA1-KI-1M) were attached to the back of the samples and connected to data logger (Pico Technology, TC-08). The ambient temperature was measured by placing the thermocouple outside the apparatus without illumination of sunlight. The thermocouples were placed inside the chamber under the shade of the Al foil to measure the chamber temperature. Solar irradiance was measured by a pyranometer (Apogee, SP-510-SS). On the testing days, the apparatus was placed on a table, elevated  $\approx 1$  m from the ground, and tilted toward the South so that sunlight was roughly normal incident on the samples at peak elevation (Figure 4b).

### Supporting Information

Supporting Information is available from the Wiley Online Library or from the author.

### Acknowledgements

This work is sponsored by Toyota Research Institute of North America and the “Photonics at Thermodynamic Limits” Energy Frontier Research



Center funded by the U.S. Department of Energy, Office of Science, Office of Basic Energy Sciences under Award Number DE-SC0019140. Research was carried out in part in the Materials Research Laboratory Central Research Facilities, University of Illinois Urbana-Champaign.

## Conflict of Interest

S. N. J., D. X., and P. V. B. have applied for a U.S. patent related to this work.

## Data Availability Statement

The data that support the findings of this study are available from the corresponding author upon reasonable request.

## Keywords

energy saving, passive thermal regulation, PNIPAM hydrogels, radiative cooling, switchable solar reflectance

Received: October 6, 2022

Published online: February 3, 2023

- [1] R. F. Rupp, N. G. Vásquez, R. Lamberts, *Energy Build.* **2015**, *105*, 178.
- [2] L. Yang, H. Yan, J. C. Lam, *Appl. Energy* **2014**, *115*, 164.
- [3] E. Rephaeli, A. Raman, S. Fan, *Nano Lett.* **2013**, *13*, 1457.
- [4] A. P. Raman, M. A. Anoma, L. Zhu, E. Rephaeli, S. Fan, *Nature* **2014**, *515*, 540.
- [5] Y. Zhai, Y. Ma, S. N. David, D. Zhao, R. Lou, G. Tan, R. Yang, X. Yin, *Science* **2017**, *355*, 1062.
- [6] J. Mandal, Y. Fu, A. C. Overvig, M. Jia, K. Sun, N. N. Shi, H. Zhou, X. Xiao, N. Yu, Y. Yang, *Science* **2018**, *362*, 315.
- [7] W. Li, S. Fan, *Opt. Express* **2018**, *26*, 15995.
- [8] T. Li, Y. Zhai, S. He, W. Gan, Z. Wei, M. Heidarinejad, D. Dalgo, R. Mi, X. Zhao, J. Song, J. Dai, *Science* **2019**, *364*, 760.
- [9] D. Li, X. Liu, W. Li, Z. Lin, B. Zhu, Z. Li, J. Li, B. Li, S. Fan, J. Xie, J. Zhu, *Nat. Nanotechnol.* **2021**, *16*, 153.
- [10] C. Lin, Y. Li, C. Chi, Y. S. Kwon, J. Huang, Z. Wu, J. Zheng, G. Liu, C. Y. Tso, C. Y. Chao, B. Huang, *Adv. Mater.* **2022**, *34*, 2109350.
- [11] S. Fan, W. Li, *Nat. Photonics* **2022**, *16*, 182.
- [12] H. Zhao, Q. Sun, J. Zhou, X. Deng, J. Cui, *Adv. Mater.* **2020**, *32*, 2000870.
- [13] J. Mandal, M. Jia, A. Overvig, Y. Fu, E. Che, N. Yu, Y. Yang, *Joule* **2019**, *3*, 3088.
- [14] P. C. Hsu, C. Liu, A. Y. Song, Z. Zhang, Y. Peng, J. Xie, K. Liu, C. L. Wu, P. B. Catrysse, L. Cai, S. Zhai, *Sci. Adv.* **2017**, *3*, e1700895.
- [15] X. Li, B. Sun, C. Sui, A. Nandi, H. Fang, Y. Peng, G. Tan, P. C. Hsu, *Nat. Commun.* **2020**, *11*, 6101.
- [16] Y. Rao, J. Dai, C. Sui, Y. T. Lai, Z. Li, H. Fang, X. Li, W. Li, P. C. Hsu, *ACS Energy Lett.* **2021**, *6*, 3906.
- [17] J. Mandal, S. Du, M. Dontigny, K. Zaghbi, N. Yu, Y. Yang, *Adv. Funct. Mater.* **2018**, *28*, 1802180.
- [18] M. Ono, K. Chen, W. Li, S. Fan, *Opt. Express* **2018**, *26*, A777.
- [19] K. Ito, T. Watari, K. Nishikawa, H. Yoshimoto, H. Iizuka, *APL Photonics* **2018**, *3*, 086101.
- [20] S. Taylor, Y. Yang, L. Wang, *J. Quant. Spectrosc. Radiat. Transfer* **2017**, *197*, 76.
- [21] K. Tang, K. Dong, J. Li, M. P. Gordon, F. G. Reichertz, H. Kim, Y. Rho, Q. Wang, C. Y. Lin, C. P. Grigoropoulos, A. Javey, *Science* **2021**, *374*, 1504.
- [22] S. Wang, T. Jiang, Y. Meng, R. Yang, G. Tan, Y. Long, *Science* **2021**, *374*, 1501.
- [23] N. A. Semenyuk, V. I. Surikov, Y. V. Kuznetsova, V. I. Surikov, V. K. Volkova, *J. Phys. Conf. Ser.* **2019**, *1260*, 062022.
- [24] Y.-X. Ji, S.-Y. Li, G. A. Niklasson, C. G. Granqvist, *Thin Solid Films* **2014**, *562*, 568.
- [25] X.-H. Li, C. Liu, S.-P. Feng, N. X. Fang, *Joule* **2019**, *3*, 290.
- [26] Y. Zhou, S. Wang, J. Peng, Y. Tan, C. Li, F. Y. C. Boey, Y. Long, *Joule* **2020**, *4*, 2458.
- [27] Y. Ke, J. Chen, G. Lin, S. Wang, Y. Zhou, J. Yin, P. S. Lee, Y. Long, *Adv. Energy Mater.* **2019**, *9*, 1902066.
- [28] C. Lin, J. Hur, C. Y. Chao, G. Liu, S. Yao, W. Li, B. Huang, *Sci. Adv.* **2022**, *8*, eabn7359.
- [29] X. Mei, T. Wang, M. Chen, L. Wu, *J. Mater. Chem. A* **2022**, *10*, 11092.
- [30] Z. Fang, L. Ding, L. Li, K. Shuai, B. Cao, Y. Zhong, Z. Meng, Z. Xia, *ACS Photonics* **2021**, *8*, 2781.
- [31] H. G. Schild, *Prog. Polym. Sci.* **1992**, *17*, 163.
- [32] A. Halperin, M. Kröger, F. M. Winnik, *Angew. Chem., Int. Ed.* **2015**, *54*, 15342.
- [33] A. Eklund, H. Zhang, H. Zeng, A. Priimagi, O. Ikkala, *Adv. Funct. Mater.* **2020**, *30*, 2000754.
- [34] Y.-S. Yang, Y. Zhou, F. B. Yin Chiang, Y. Long, *RSC Adv.* **2016**, *6*, 61449.
- [35] D. Coker, J. Reimers, R. Watts, *Aust. J. Phys.* **1982**, *35*, 623.
- [36] J. Zheng, P. Xiao, X. Le, W. Lu, P. Théato, C. Ma, B. Du, J. Zhang, Y. Huang, T. Chen, *J. Mater. Chem. C* **2018**, *6*, 1320.
- [37] Y. Brasse, M. B. Müller, M. Karg, C. Kuttner, T. A. König, A. Fery, *ACS Appl. Mater. Interfaces* **2018**, *10*, 3133.
- [38] G. M. Hale, M. R. Querry, *Appl. Opt.* **1973**, *12*, 555.
- [39] T. Kaino, in *Encyclopedia of Polymeric Nanomaterials* (Eds: S. Kobayashi, K. Müllen), Springer, Berlin, Heidelberg **2014**, pp. 1–14, [https://doi.org/10.1007/978-3-642-36199-9\\_118-1](https://doi.org/10.1007/978-3-642-36199-9_118-1).
- [40] G. A. Carter, D. C. McCain, *Remote Sens. Environ.* **1993**, *46*, 305.
- [41] H. Du, R. Wickramasinghe, X. Qian, *J. Phys. Chem. B* **2010**, *114*, 16594.
- [42] Y. Zhang, S. Furyk, D. E. Bergbreiter, P. S. Cremer, *J. Am. Chem. Soc.* **2005**, *127*, 14505.
- [43] R. O. R. Costa, R. F. S. Freitas, *Polymer* **2002**, *43*, 5879.
- [44] C. H. Lee, Y. C. Bae, *Polymer* **2020**, *195*, 122428.
- [45] T. E. de Oliveira, D. Mukherji, K. Kremer, P. A. Netz, *J. Chem. Phys.* **2017**, *146*, 034904.
- [46] G. E. Walrafen, in *The Physics and Physical Chemistry of Water* (Ed: F. Franks), Springer, New York **1972**, pp. 151–214, [https://doi.org/10.1007/978-1-4684-8334-5\\_5](https://doi.org/10.1007/978-1-4684-8334-5_5).
- [47] Y. Shi, W. Li, A. Raman, S. Fan, *ACS Photonics* **2018**, *5*, 684.
- [48] J. A. Lustbader, C. Kreutzer, M. Jeffers, S. Adelman, S. Yeakel, P. Brontz, K. Olson, J. Ohlinger, *Impact of Paint Color on Rest Period Climate Control Loads in Long-Haul Trucks* **2014**, SAE Technical Paper 2014-01-0680, <https://doi.org/10.4271/2014-01-0680>.
- [49] A. Baniassadi, D. J. Sailor, P. J. Crank, G. A. Ban-Weiss, *Energy Build.* **2018**, *178*, 71.
- [50] K. Zhou, N. Miljkovic, L. Cai, *Energy Build.* **2021**, *235*, 110749.